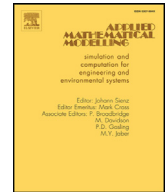


Contents lists available at [ScienceDirect](http://www.sciencedirect.com)

Applied Mathematical Modelling

journal homepage: www.elsevier.com/locate/apm

Conservative 1D–2D coupled numerical strategies applied to river flooding: The Tiber (Rome)[☆]

M. Morales-Hernández^{a,*}, G. Petaccia^b, P. Brufau^a, P. García-Navarro^a^a Fluid Mechanics, LIFTEC-EINA, CSIC-Universidad de Zaragoza, Zaragoza, Spain^b Department of Civil Engineering and Architecture, University of Pavia, Pavia, Italy

ARTICLE INFO

Article history:

Received 26 November 2013

Revised 13 April 2015

Accepted 26 August 2015

Available online xxx

Keywords:

1D–2D coupled model

Shallow water

Conservation

River flooding

ABSTRACT

Coupled 1D–2D numerical strategies are presented in this work for their application to fast computation of large rivers flooding. Both 1D and 2D models are built using explicit upwind finite volume schemes, able to deal with wetting–drying fronts. The topography representation is described via cross sections for the 1D model and with quadrilateral/triangular structured/unstructured meshes for the 2D model. The coupling strategies, free of hydraulic structures and tuning parameters, are firstly validated in a laboratory test dealing with a levee break and its flooding into a lateral plane. The numerical results are compared with a fully 2D model as well as with measurements in some gauge points giving satisfactory results. The simulation of a real flooding scenario in the Tiber river near the urban area of Rome (Italy) is then performed. A lateral coupling configuration is provided, in which the flood wave propagation in the main channel is simulated by means of a 1D model and the inundation of the riverside is simulated by means of a 2D model. On the other hand, a frontal coupling, in which the flood wave is simulated in a 1D model first and then it is propagated into a 2D model, is also performed. The flooding extension is almost well captured by all the schemes presented, being the 1D–2D lateral configuration the most confident with speed-ups of around 15x.

© 2015 Elsevier Inc. All rights reserved.

1. Introduction

Environmental hazards associated to flooding events near urban areas are becoming a growing problem. Modern flood risk management and mitigation plans incorporate the presence of numerical models that are able to assess the response of the system and to help in the decision-making processes. However, the advances in computers are not sufficient to run the simulations as fast as desired and new models are demanded in order to cover all the possible scenarios in large temporal and spatial scales. Hydraulic models can be classified according to the number of dimensions in which they represent the spatial domain as 1D, 2D or 3D. In particular, 3D approaches may not be adequate given the available information, basically topography, local water depth measurements and observed flooded area extension. For that reason, 1D and 2D models are preferred. The Shallow Water Equations (SWE) allow to model the flooding phenomena. 1D SWE models are usually adopted when simulating long rivers and open channel flows [1,8,20,35,36,38,40] due to their computational efficiency, particularly for river network systems. However, they are unable to approximate correctly the behavior in floodplains. On the contrary, 2D SWE models are valid when

[☆] The authors would like to dedicate this article to the late researcher F. Savi, Department of Hydraulics, Transportation and Highways, La Sapienza University, Rome, Italy for his fruitful contributions and support for this work.

* Corresponding author. Tel.: +34 976 555052.

E-mail address: mmorales@unizar.es, pol_mmh@hotmail.com (M. Morales-Hernández).

<http://dx.doi.org/10.1016/j.apm.2015.08.016>

S0307-904X(15)00537-5/© 2015 Elsevier Inc. All rights reserved.

Please cite this article as: M. Morales-Hernández et al., Conservative 1D–2D coupled numerical strategies applied to river flooding: The Tiber (Rome), Applied Mathematical Modelling (2015), <http://dx.doi.org/10.1016/j.apm.2015.08.016>

modeling complex not canalized flows as floodplains [5,7,13] nevertheless the large amount of computations required in real world applications make them very time consuming and unaffordable in real time simulations.

To overcome these difficulties, coupled models can be adopted. Although coupled 1D–3D models have been developed recently for simulating the interaction between rivers and oceans [12], 1D–2D models are still widely popular. The first simplified 1D–quasi 2D model dates to 1975 with the Mekong river delta model [14], where a 1D model of looped channel flow, solving the SWE with the Preissmann scheme, was integrated with a storage cell algorithm using the mass conservation equation to link domains. The storage cell approach was later adopted also by Bladé et al. [4] on academic test cases. In a similar way Kuiry et al. [23] applied a simplified 1D–quasi 2D model to a stretch of River Severn, solving 1D SWE in the river channel and using a storage cell method to compute the overbank flow. The exchange between 1D and 2D models is represented by the diffusive wave approximated equation. Villanueva and Wright integrated a 1D model with two 2D models [39], the first based on a storage cell approach and the second on a Riemann solver. These models are linked via spills between the main channel and the floodplain with mass transfer. In [29], two strategies are reviewed to improve urban flood forecasting. The first consists of a simplification of the mathematical formulation using an efficient 2D raster storage cell approach coupled to a 1D channel model. The second one uses a sub-grid parametrization to represent the effects of buildings and micro topography on flow pathways and floodplain storage. The two strategies are evaluated through a numerical experiment designed to reconstruct a flood in the city of Linton, England. Castellarin et al. developed and tested the applicability of a quasi 2D hydraulic model [9] to aid the identification of large scale flood risk mitigation strategies. This approach considers the interaction between the channel and the floodplains only by mass transfer, completely neglecting the momentum exchange.

In most of the proposed 1D–2D models, the connection is formulated by means of a lateral weir equation [15,38] in which the exchanged volume is governed by surface level differences [26]. The same idea was applied in [21] to solve a levee break. The authors coupled a full 1D model based on SWE solved by Preissman method with a 2D model which solves the diffusion wave equation by a finite difference method. The overflow through the broken levee is treated as an internal boundary condition. Yin et al. [41] coupled a 1D solution of the full form of the SWE and a 2D floodplain flow model to predict the Huangpu river flood and inundation extents. In [16], the hybrid methodology was also used on a 28 km reach of Reno River: flows through the lateral weir and simulated breaches were computed by a 1D approach and then adopted as the inflow boundary condition for a 2D model of the flood-prone area. Horritt and Bates [22] compare two approaches to model floodplain inundation: a raster-based approach, with channel flow being resolved separately from the floodplain using either a kinematic or diffusive wave approximation, and a finite-element hydraulic model aiming to solve the full 2D SWE. The approaches are tested on a flood event on a short reach of the upper River Thames in the UK, and are validated against inundation extent as determined from satellite synthetic aperture radar (SAR) imagery. Masoero et al. [28] apply a similar approach to compute the flow through the levee breach of the river Po.

Miglio et al. [30] applied an iterative procedure to solve the coupled 1D–2D problem after transforming the 2D variables into 1D integrated quantities and imposing continuity at the interfaces. This technique turns out to be a reliable strategy provided that a proper choice of the subdomain is performed, only for simple configurations (e.g. a straight channel or a river bifurcation). Yu and Lane [42] propose a loosely coupled approach where the 1D model is used to provide boundary conditions to the 2D model at the floodplain interface prior to the initialization of the 2D model. This study showed that, if the exchange between river and floodplain is not represented correctly, it is likely that flood inundation extent will not be modeled correctly. The importance of boundary conditions for flood inundation predictions is also emphasized.

The idea of a locally zoom model superimposed over an open channel network global model is elaborated in [17,19]. The zoom model (2D SWE) describes additional physical phenomena which are not represented by the global model (1D SWE). The application of this model is only shown for toy test cases. The same model was further developed in [27] showing results for simple test cases.

Recent research has advanced in exploring 1D–2D coupling strategies to combine the best attributes of each model. In [18], a coupled 1D–2D model was presented, in which the momentum transfer between the main channel and the floodplain is taken into account. The model is first applied to simple test cases and then to a real world configuration. Also a coupling approach of a 1D and a 2D model working in subcritical conditions is found in [11].

A numerical method for coupling full 1D and 2D finite volume scheme is presented by Morales-Hernández et al. [31]. The linking between the two models is pursued by exchanging the necessary information to achieve a fully conservative 1D–2D coupled model, considering the information that leaves out each computational domain and its connection to the boundary conditions. In that preliminary work, the performance of the coupled model was evaluated in academic test cases specifically designed to check the influence of the flow regime at the coupling zone.

In the present work, an extension of [31] to realistic problems of interest in engineering is explored. The topography is usually described by means of cross sections in the main channel of a river and with DEM (Digital Elevation Model) over the floodplain. These two sets of data do not always match perfectly. Instead, they overlap in some regions or generate gaps in others [10]. Our effort has been devoted to obtain the best topography representation required by all the models. In particular, left and right bank limits have to be identified in the cross sections to enable the connection with the 2D floodplain when facing a lateral coupling. Moreover, a careful and detailed surface level/water volume is required at the coupling zone to ensure the success of the proposed coupling strategy.

Both models are implemented using a single finite volume framework based on an explicit first order upwind numerical scheme [6]. The way of coupling the 1D and 2D hydrodynamical models can be frontal or lateral and is presented according to [31]. The 2D computation can be performed over structured/unstructured triangular and squared meshes and this possibility will be illustrated.

The main objective of this work is to stress the capability of the proposed 1D–2D coupled model in flood applications. After this introduction, the governing equations as well as the numerical scheme are detailed. The 1D–2D coupled model is outlined, with special emphasis on the connection between the models. Then, one laboratory experimental test case corresponding to a levee break in a channel propagating into a lateral flood plain [3] has been simulated and then the coupled model is applied to a real flood in the Tiber River, Italy. Numerical results of the 1D–2D coupled model are compared with those obtained with fully 2D schematization as well as with field measurements.

2. Governing equations

2.1. 1D shallow water equations

The 1D shallow water equations express the conservation of mass and momentum in the longitudinal direction and can be written in conservative form as follows:

$$\frac{\partial \mathbf{U}(x, t)}{\partial t} + \frac{d\mathbf{F}(x, \mathbf{U})}{dx} = \mathbf{H}(x, \mathbf{U}) \quad (1)$$

$$\mathbf{U} = \begin{pmatrix} A \\ Q \end{pmatrix}, \quad \mathbf{F} = \begin{pmatrix} Q \\ \frac{Q^2}{A} + gI_1 \end{pmatrix}, \quad \mathbf{H} = \begin{pmatrix} 0 \\ g[I_2 + A(S_0 - S_f)] \end{pmatrix} \quad (2)$$

where Q is the discharge, A is the wetted area, g is the acceleration due to the gravity, S_0 accounts for the bed variations

$$S_0 = -\frac{\partial z_b}{\partial x} \quad (3)$$

and S_f represents the friction losses modeled by means of the empirical Manning–Strickler formula:

$$S_f = \frac{Q^2 n^2}{A^2 R^{4/3}} \quad (4)$$

being n the Manning's roughness coefficient. In this work, the hydraulic radius R has been chosen as $R = \frac{A}{B}$ where B is the top width surface. This fact allows to homogenize the meaning of the roughness coefficient n in both the 1D and the 2D models. I_1 and I_2 account for hydrostatic and longitudinal width variation pressure forces respectively:

$$I_1 = \int_{z_b}^{z_s} (h - \eta) \sigma(x, \eta) d\eta \quad (5)$$

$$I_2 = \int_{z_b}^{z_s} (h - \eta) \frac{\partial \sigma(x, \eta)}{\partial x} d\eta \quad (6)$$

where z_s is the water level, z_b is the bed level and $\sigma(x, \eta)$ is the width of the cross section. It is feasible to derive the non-conservative system of equations from Eqs. (1) and (2), considering the following remark [8,31]:

$$\frac{d\mathbf{F}(x, \mathbf{U})}{dx} = \frac{\partial \mathbf{F}(x, \mathbf{U})}{\partial x} \Big|_{\mathbf{U}=\text{const}} + \frac{\partial \mathbf{F}(x, \mathbf{U})}{\partial \mathbf{U}} \Big|_{x=\text{const}} \frac{\partial \mathbf{U}(x, t)}{\partial x} \quad (7)$$

Therefore, 1D shallow water equations can be written accordingly:

$$\frac{\partial \mathbf{U}(x, t)}{\partial t} + \frac{\partial \mathbf{F}(x, \mathbf{U})}{\partial x} \Big|_{x=\text{const}} = \mathbf{H}'(x, \mathbf{U}) \quad (8)$$

where $\mathbf{H}'(x, \mathbf{U})$ represents the vector related with the sources, expressed in the non-conservative form:

$$\mathbf{H}'(x, \mathbf{U}) = \mathbf{H}(x, \mathbf{U}) - \frac{\partial \mathbf{F}(x, \mathbf{U})}{\partial x} \Big|_{\mathbf{U}=\text{const}} \quad (9)$$

2.2. 2D shallow water equations

The depth averaged mass and momentum conservation are expressed as follows for the 2D shallow water equations:

$$\frac{\partial \mathbf{U}}{\partial t} + \frac{\partial \mathbf{F}(\mathbf{U})}{\partial x} + \frac{\partial \mathbf{G}(\mathbf{U})}{\partial y} = \mathbf{H}(\mathbf{U}) \quad (10)$$

where \mathbf{U} are the conserved variables:

$$\mathbf{U} = (h, q_x, q_y)^T \quad (11)$$

and \mathbf{F}, \mathbf{G} are the fluxes of these variables:

$$\mathbf{F} = \left(q_x, \frac{q_x^2}{h} + \frac{1}{2}gh^2, \frac{q_x q_y}{h} \right)^T, \quad \mathbf{G} = \left(q_y, \frac{q_x q_y}{h}, \frac{q_y^2}{h} + \frac{1}{2}gh^2 \right)^T \quad (12)$$

being h the water depth and q_x and q_y the unit discharges in x and y components, respectively. The vector of source terms in (10) includes the presence of bed and friction slopes

$$\mathbf{H} = (0, gh(S_{0x} - S_{fx}), gh(S_{0y} - S_{fy}))^T \quad (13)$$

where the bed variations of the bottom level z in x and y directions are

$$S_{0x} = -\frac{\partial z_b}{\partial x}, \quad S_{0y} = -\frac{\partial z_b}{\partial y} \quad (14)$$

and the friction slope is expressed, as in the 1D model, in terms of the Manning's roughness coefficient n :

$$S_{fx} = \frac{n^2 u \sqrt{u^2 + v^2}}{h^{4/3}}, \quad S_{fy} = \frac{n^2 v \sqrt{u^2 + v^2}}{h^{4/3}} \quad (15)$$

3. Numerical scheme

In this work, the focus is put on upwind first order finite volume schemes for both 1D and 2D models. Although the common practice in CFD models is to use high order (at least second order) schemes, in flood propagation modelling first order schemes are sufficient [33,34]. The main reason is that in the majority of the flows concerning realistic applications, the source terms dominate over the convective terms. Therefore, the use of second order schemes is not always justified by the increase in computational costs as the focus is put on the correct balance of fluxes and source terms. Both 1D and 2D systems of conservation laws can be written compactly:

$$\frac{\partial \mathbf{U}}{\partial t} + \vec{\nabla} \mathbf{E} = \mathbf{S} \quad (16)$$

where $\mathbf{E} = \mathbf{F}$ and $\mathbf{S} = \mathbf{H}'$ in the 1D model and $\mathbf{E} = (\mathbf{F}, \mathbf{G})$ and $\mathbf{S} = \mathbf{H}$ in the 2D case. In order to derive the finite volume scheme, this equation is integrated in a computational cell Ω :

$$\frac{\partial}{\partial t} \int_{\Omega} \mathbf{U} d\Omega + \int_{\Omega} (\vec{\nabla} \mathbf{E}) d\Omega = \int_{\Omega} \mathbf{S} d\Omega \Rightarrow \frac{\partial}{\partial t} \int_{\Omega} \mathbf{U} d\Omega + \oint_{\partial\Omega} \mathbf{E} \mathbf{n} dm = \int_{\Omega} \mathbf{S} d\Omega \quad (17)$$

where \mathbf{n} denotes the outward normal vector to the cell. The Jacobian \mathbf{J}_n of the normal flux $\mathbf{E} \mathbf{n}$ can be diagonalized in terms of the diagonal matrix Λ_n , formed by its eigenvalues and \mathbf{P} , containing its eigenvectors:

$$\mathbf{J}_n = \mathbf{P} \Lambda_n \mathbf{P}^{-1}, \quad \Lambda_n = \mathbf{P}^{-1} \mathbf{J}_n \mathbf{P} \quad (18)$$

Roe's linearization [37] is used to decouple the original hyperbolic system (15) and to define locally an approximate matrix $\tilde{\mathbf{J}}_n$ at each interface k . Denoting i and j the neighboring cells sharing this interface k , the differences in the vector of conserved variables \mathbf{U} across k can be written in terms of the linearized eigenvectors basis $\tilde{\mathbf{e}}^m$:

$$\delta \mathbf{U}_k = \mathbf{U}_i - \mathbf{U}_j = \sum_m (\tilde{\alpha} \tilde{\mathbf{e}})_k^m \quad (19)$$

The vector of source terms is also projected onto the eigenvectors basis and discretized following the upwind philosophy:

$$\mathbf{S}_k = \sum_m (\tilde{\beta} \tilde{\mathbf{e}})_k^m \quad (20)$$

The explicit first order upwind numerical scheme for the 1D model can be expressed as follows [8,31]:

$$\mathbf{U}_i^{n+1} = \mathbf{U}_i^n - \frac{\Delta t_{1D}}{\delta x} \left[\left(\sum_m \tilde{\lambda}^+ \tilde{\gamma} \tilde{\mathbf{e}} \right)_{i-1/2}^m + \left(\sum_m \tilde{\lambda}^- \tilde{\gamma} \tilde{\mathbf{e}} \right)_{i+1/2}^m \right]^n \quad (21)$$

where $m = 2$, $k = 2$, $i + 1/2$ denotes the interface between cells i and $i + 1$ (analogous with $i - 1/2$ and cells $i - 1$ and i), $\tilde{\gamma}_{i+1/2}^m = (\tilde{\alpha} - \frac{\tilde{\beta} \delta x}{\tilde{\lambda}})_{i+1/2}^m$ and $\tilde{\lambda}_{i+1/2}^{\pm m} = \frac{1}{2} (\tilde{\lambda} \pm |\tilde{\lambda}|)_{i+1/2}^m$. The time step size is restricted by the Courant–Friedrich–Lewy condition:

$$\Delta t_{1D} = CFL \frac{\delta x}{\max_{m,i} |\tilde{\lambda}^m|_i} \quad CFL \leq 1 \quad (22)$$

where CFL is the Courant number.

The formulation of the 2D first order upwind explicit scheme is completely equivalent to the 1D model [6,7,32]:

$$\mathbf{U}_i^{n+1} = \mathbf{U}_i^n - \frac{\Delta t_{2D}}{S_i} \sum_{k=1}^{NE} \sum_m [(\tilde{\lambda}^- \tilde{\gamma} \tilde{\mathbf{e}})_k^m l_k]^n \quad (23)$$

This expression shows that the conserved variables from time n to time $n + 1$ will be updated according to the contributions that arrive from the neighboring walls to the cell i with area S_i . In the 2D model, $m = 3$, NE is the number of neighboring cells

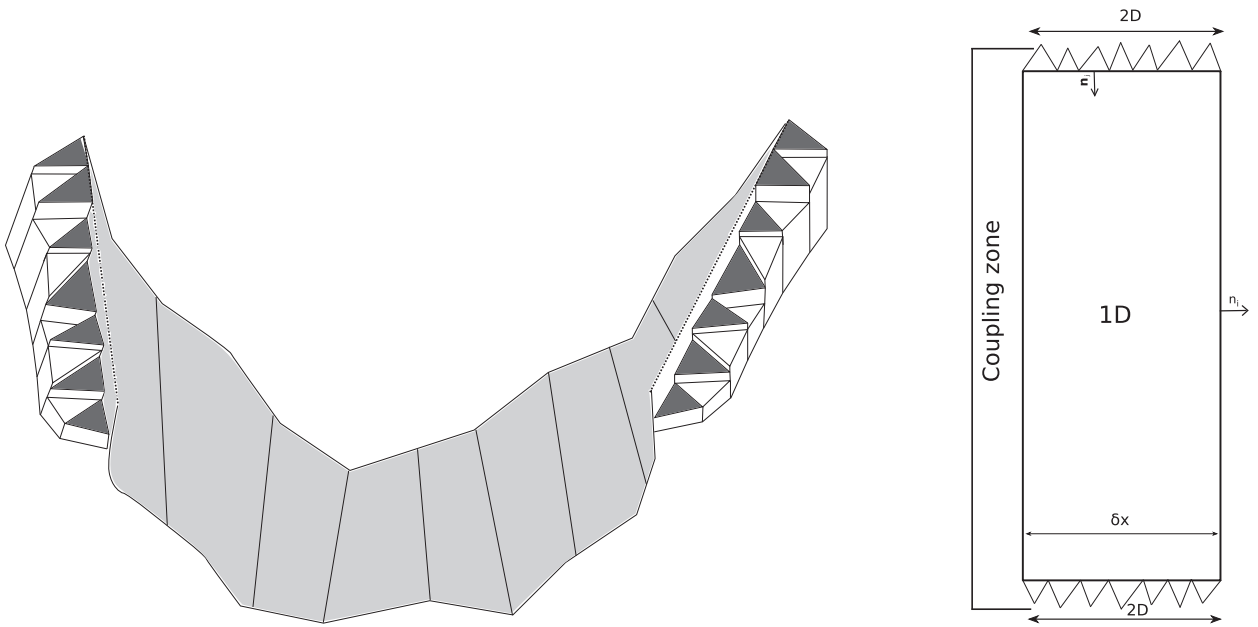


Fig. 1. Lateral coupling zone in a river: 3D view (left) and plant view (right).

($NE = 3$ in the case of triangular grids, $NE = 4$ for squared grids) and l_k is the length of each interface. The time step is again limited by the CFL condition

$$\Delta t_{2D} = CFL \frac{\min(\chi_i, \chi_j)}{\max_m |\tilde{\lambda}^m|} \quad CFL \leq 1 \quad (24)$$

where χ_i represents a characteristic distance of cell i and its k neighboring edges, necessary when dealing with unstructured triangular grids:

$$\chi_i = \frac{S_i}{\max_{k=1,NE} l_k} \quad (25)$$

It is worth remarking that both 1D and 2D numerical schemes have proved to be conservative, well-balanced and positivity preserving when used separately [8,32].

4. 1D–2D coupled model

The 1D and 2D numerical schemes presented above are coupled by means of the fully conservation property [31]. For that purpose, it is feasible to define a new element of discretization in which the 1D and the 2D cells can interact: the *coupling zone*. It is constituted by one 1D cell and N_c 2D adjacent computational cells hence a good meshing procedure is required to ensure this fulfilment. Thereupon, two configurations appear naturally with respect to the 1D model: frontal and lateral. In particular, Fig. 1 displays a lateral coupling zone in a complex river with uneven bathymetry in a 3D view (left) and its representation in plant (right).

The mentioned coupling zones are constructed in the pre-process and subsequently the set of initial conditions for each model is applied. Once the computation starts, and for each iteration, a suitable time step size is essential to handle the interaction between the models. As seen before, each model has its own time step size that comes from their corresponding stability conditions. Therefore, in order to homogenize it, a global Δt is selected as the minimum value of the two models:

$$\Delta t = \min(\Delta t_{1D}, \Delta t_{2D}) \quad (26)$$

Once the time step size is established, each model runs independently according to (21) and (23), respectively, that is, without interacting between them. The new conserved variables provided by each numerical scheme, denoted from now on with a superscript star *, are used to link both models. Depending on which strategy (only mass conservation or mass and momentum conservation) is imposed, the models will exchange the required information at each coupling zone and will update its own conserved variables with the new states to move forward to the following time step. Fig. 2 summarizes the flowchart followed in this work for the 1D–2D coupled model.

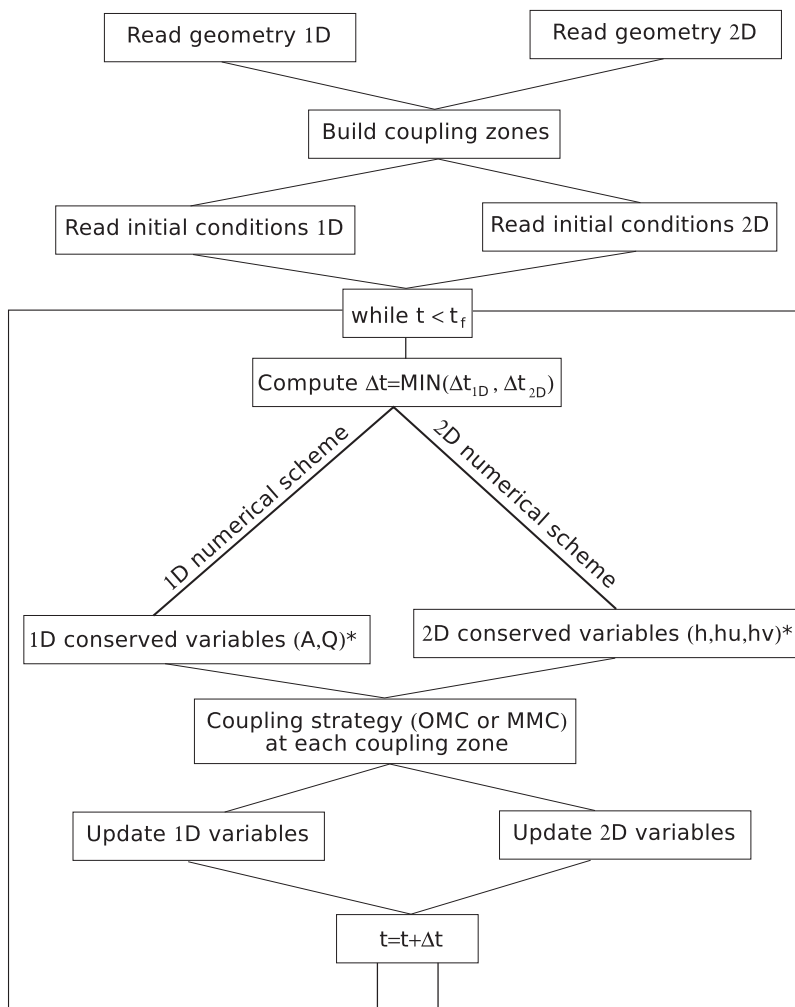


Fig. 2. Flowchart of the 1D–2D coupled scheme.

4.1. Exchanging the information between the models: coupling strategies

In the frontal configuration, the 1D and the 2D models will always exchange information provided they are wet. On the opposite, in the lateral configuration, both models will obviously interact only when a flooding at the coupling zone is registered, whether by the 1D model or by the 2D model. Consequently, it is necessary to establish an ‘overflow level’ for each lateral coupling zone, which will be split into two levels (left overflow and right overflow). In this work, a simple linear interpolation between the extreme left and right points of the each 1D cross section is established as the left and right overflow levels respectively. Four possibilities arise:

- **No overflow.** There is not interaction between the models (Fig. 3 (a)).
- **Left overflow.** The models exchange information between the 1D cell and the 2D adjacent cells which are on the left side of the coupling zone (Fig. 3 (b)).
- **Right overflow.** The models exchange information between the 1D cell and the 2D adjacent cells which are on the right side of the coupling zone (Fig. 3 (c)).
- **Left and right overflow.** The models exchange information between the 1D cell and all the 2D adjacent cells involved at the coupling zone (Fig. 3 (d)).

If an overflow occurs at the coupling zone, both models must interact and, in this work, two approaches are proposed based on a fully mass conservation or mass and momentum conservation respectively. The Only Mass Conservation (OMC) consists of imposing a joint water surface level at each the coupling zone. In order to be able to adapt the variables provided by each model, the total water volume at the coupling zone is evaluated. However, it is not only a question of accounting for the amount of water present at the corresponding time inside the coupling zone, but also the discharge integrated in time that crossed the boundary

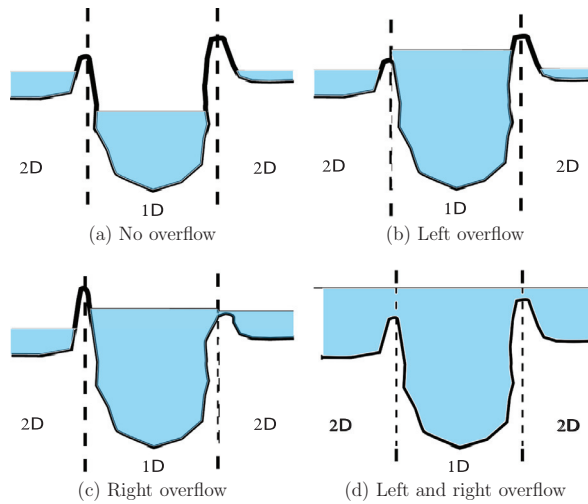


Fig. 3. Possibilities for the interaction between the 1D and the 2D models in a lateral configuration.

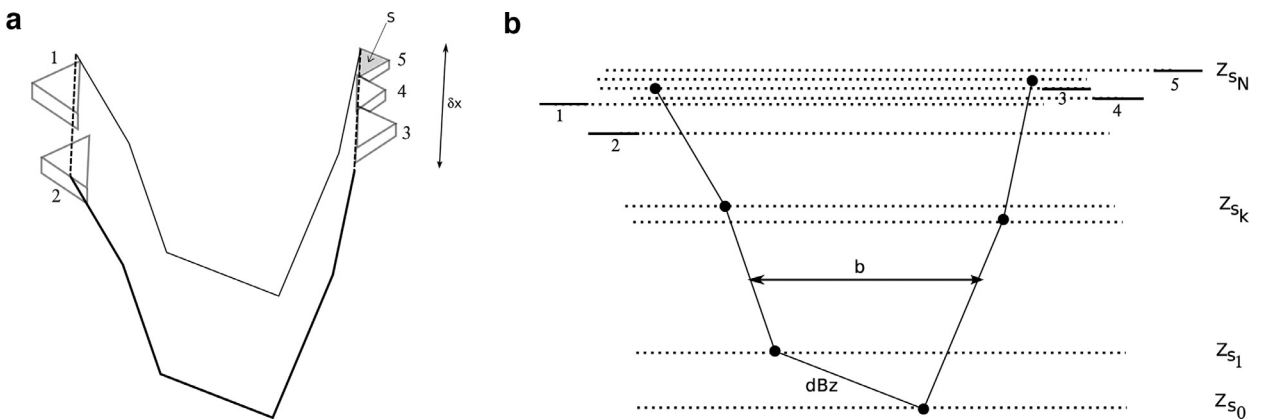


Fig. 4. Coupling zone (a) and sliced sketch (b).

edges separating the two models. Therefore, the total volume of the coupling zone, V_{CZ} holds:

$$V_{CZ} = A_{1D}^* \delta x + \sum_i^{N_c} h_i^* S_i + Q_{1D}^n n_{1D} \Delta t + \sum_i^{N_c} (\mathbf{F}_{1i}^n \cdot \mathbf{n}_i l_i) \Delta t \quad (27)$$

where $\mathbf{F}_{1i}^n = (q_x, q_y)$, l_i the length of each boundary edge shared by the 1D and 2D domains at the corresponding coupling zone and \mathbf{n}_i the outward normal direction to the 2D cell (see Fig. 1, right). It is worth clarifying that $n_{1D} = 0$ in the lateral coupling while $n_{1D} = \pm 1$ in the frontal coupling configuration. The meaning of Eq. (27) condense indeed the strict mass conservation property: the volume of water of the 1D model, $A_{1D}^* \delta x$, of the 2D model, $\sum_i^{N_c} h_i^* S_i$, as well as the 1D-flow, $Q_{1D}^n n_{1D} \Delta t$, and the 2D-flow, $\sum_i^{N_c} (\mathbf{F}_{1i}^n \cdot \mathbf{n}_i l_i) \Delta t$, that cross the edges between the two models.

The same water level surface, z_s^{n+1} is enforced at the coupling zone. Thus, it is necessary to distribute appropriately the volume V_{CZ} in both 1D and 2D models with the aid of level-volume tables, built in the pre-process for each coupling zone, that are able to deal with complex topography.

Let consider a coupling zone as in Fig. 4 (a), composed by one 1D irregular cell, two coupled 2D cells called 1 and 2 on the left side and three coupled 2D cells called 3, 4 and 5, respectively on the right side. Fig. 4 (b) shows a sliced sketch of the mentioned coupling zone, where the straight lines represent the bottom or elevation of the corresponding 2D coupled cells.

First of all, it is necessary to construct a vector of N levels z_{s_k} , where N represents the sum of the 1D points defining the irregular cross sections for the 1D model as well as the elevation of the 2D coupled cells. Then, this vector of levels is sorted from lower to higher and a table with the information included in (28)

$$z_{s_k} \quad b_k \quad S_k \quad dBz_k \quad V_k \quad (28)$$

must be filled. As displayed in Fig. 4, k indicates the vector index, z_s is the surface level, b is the corresponding width in the 1D model, S includes the accumulated 2D cell sizes, dBz is the corresponding side slopes and V is the water volume. While the

construction of z_{s_k} , b_k , S_k and dBz_k is a straightforward geometric procedure, the volume is achieved following the rule:

$$V_{k+1} = V_k + C_k(z_{s_{k+1}} - z_{s_k}) + \frac{1}{2}dBz_k\delta x (z_{s_{k+1}} - z_{s_k})^2 \quad (29)$$

being δx the 1D cell size and $C = b\delta x + S$. During the computation, a water volume V_{CZ} is achieved from (27) at the coupling zone, that will be associated to a correct level z_s^{n+1} . In order to do this assignment, the second order (in z_s^{n+1}) Eq. (30) should be solved:

$$V_{CZ} = V_j + C_j(z_s^{n+1} - z_{s_j}) + \frac{1}{2}dBz_j\delta x (z_s^{n+1} - z_{s_j})^2 \quad (30)$$

where j is the index corresponding to V_j , immediately below V_{CZ} in the table (28). Finally, the unique solution for z_s^{n+1} satisfying

$$z_{s_j} \leq z_s^{n+1} \leq z_{s_{j+1}} \quad (31)$$

is imposed as the desired water surface level. Finally, the models, supplied with this common water level surface, update its own conserved variables as follows:

$$A_{1D}^{n+1} = A_{1D}^{n+1}(z_s^{n+1}) \quad h_i^{n+1} = z_s^{n+1} - z_{b_i} \quad (32)$$

The second strategy is called Mass and Momentum Conservation (MMC) and can be considered as an extension of the OMC strategy, in which not only a common level surface at the coupling zone is imposed but also the velocities in x and y direction. The 1D discharge, Q_{1D} , has to be converted into a vector with a flow angle θ

$$Q_{1D} \rightsquigarrow (Q_{x1D}, Q_{y1D}) = (Q_{1D} \cos \theta, Q_{1D} \sin \theta) \quad (33)$$

which allow to bidimensionalize the 1D discharge into the 2D space. For instance, in a channel completely oriented to the x -direction (assume the flow goes from left to right), $\theta = 0$ while in a channel oriented to the y -direction (the flow goes from upper to lower), $\theta = -\pi/2$. In a complex river, the thalweg or centerline of the river has to be computed in order to sample the normal direction along this thalweg. Therefore, different θ 's will be computed for different coupling zones (depending of the river orientation in the 2D space).

Consequently, the idea of a strict conservation (previously explained for the water volume) can be applied to the momentum in the x direction:

$$M_x = Q_{x1D}^* \delta x + \sum_i^{N_c} (q_x)_i^* S_i + E_x^n n_{1D} \Delta t + \sum_i^{N_c} (\mathbf{F}_{2i}^n \cdot \mathbf{n}_i l_i) \Delta t \quad (34)$$

and in the y -direction:

$$M_y = Q_{y1D}^* \delta x + \sum_i^{N_c} (q_y)_i^* S_i + E_y^n n_{1D} \Delta t + \sum_i^{N_c} (\mathbf{F}_{3i}^n \cdot \mathbf{n}_i l_i) \Delta t \quad (35)$$

where

$$\begin{aligned} \mathbf{E}_{1D}^n &= (E_x, E_y)_{1D}^n = \left(\frac{(Q_x)^2}{A} + gI_1, \frac{(Q_y)^2}{A} + gI_1 \right)_{1D}^n \\ \mathbf{F}_{2i}^n &= \left(\frac{q_x^2}{h} + \frac{1}{2}gh^2, \frac{q_x q_y}{h} \right)_i^n \quad \mathbf{F}_{3i}^n = \left(\frac{q_x q_y}{h}, \frac{q_y^2}{h} + \frac{1}{2}gh^2 \right)_i^n \end{aligned} \quad (36)$$

It is important to notice again that $n_{1D} = 0$ in the pure lateral coupling and $n_{1D} = \pm 1$ in the frontal configuration. As the water volume V_{CZ} has been previously computed, average velocities \bar{u} and \bar{v} in x and y direction can be deduced from:

$$V_{CZ} \bar{u} = M_x \quad V_{CZ} \bar{v} = M_y \quad (37)$$

With this information, the conserved variables are updated:

$$(q_x)_i^{n+1} = h_i^{n+1} \bar{u} \quad (q_y)_i^{n+1} = h_i^{n+1} \bar{v} \quad (38)$$

$$Q_{1D}^{n+1} = A_{1D}^{n+1} (\bar{u} \cos \theta + \bar{v} \sin \theta) \quad (39)$$

The imposition of Only Mass Conservation (OMC) and Mass and Momentum Conservation (MMC) is not a simple task and, in particular, boundary conditions play an important role. As an illustration, the 2D domain always ends up at each coupling zone in a lateral coupling configuration. In fact, the imposition of the OMC or MMC strategy is certainly related to the number of boundary conditions needed for each model when facing up to subcritical or supercritical flow [31]. Therefore, the Froude number is computed locally at each coupling zone and for each model:

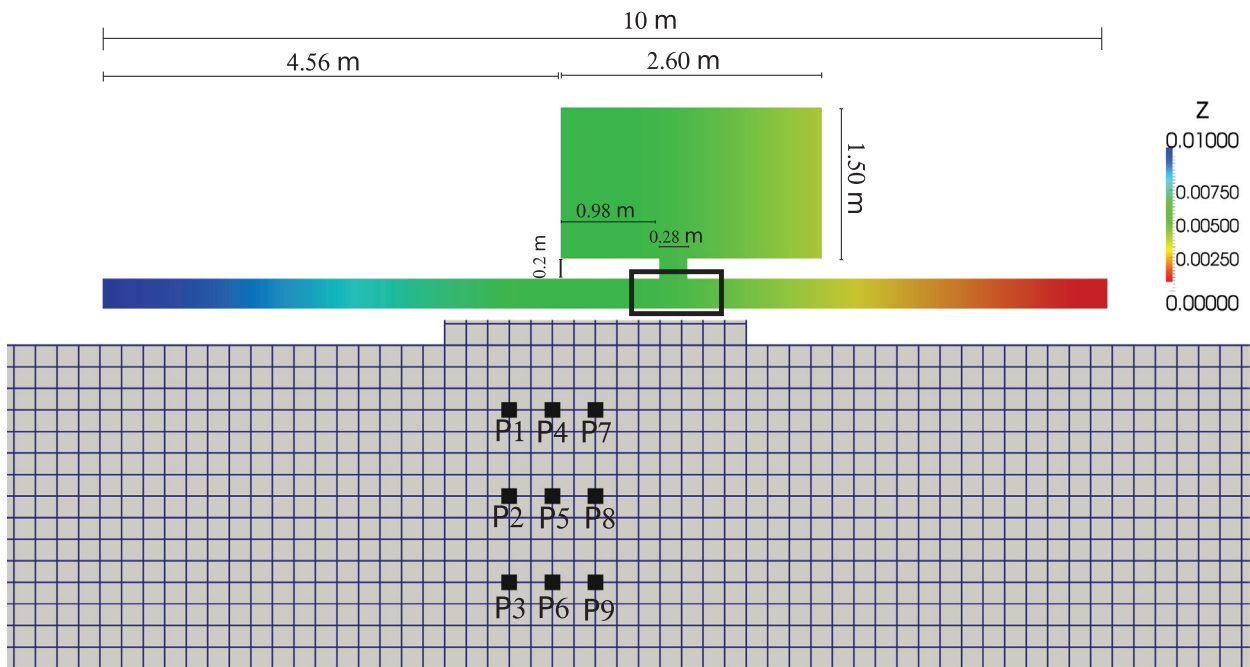


Fig. 5. Laboratory test case. Full set-up (upper) and detail of the squared mesh and the location of the probes (lower).

$$Fr_{1D} = \left(\frac{Q}{A \sqrt{g \frac{A}{B}}} \right)_{1D} \quad \overline{Fr}_{2D} = \frac{1}{N_C} \sum_i^{N_C} Fr_i \quad (40)$$

If the flow is supercritical, i.e., $Fr_{1D} > 1.0$ or $\overline{Fr}_{2D} > 1.0$, MMC is enforced. Otherwise, the OMC technique is used. Therefore, the MMC strategy is designed so that it reduces automatically to the OMC when less boundary conditions have to be imposed at the coupling zone. Indeed, the MMC strategy seems a priori to be more sophisticated than OMC due to the fact that it is being exchanging information not only related to the mass in both 1D and 2D models but also related to the momentum. However, when dealing with subcritical flow at the coupling zone, only one variable (the common water level surface, OMC strategy) has to be imposed. Otherwise, if enforcing the MMC technique, more information than necessary is provided so that the system is “overdetermined” in a certain way and may produce non-physical results [31]. In conclusion, the corresponding strategy (OMC or MMC) is dynamically and locally chosen according to the discrete flow regime at each coupling zone.

5. Laboratory test case: levee breaking in a channel with a flood plain

A test case measured in a laboratory is presented for the validation of the numerical strategies proposed in the above sections. It consists of a levee breaking test in which the inundation area is initially dry. This experiment was performed in the Parma University laboratory [3]. The experimental facility consisted of a laboratory flume (10 m long and 0.30 m wide) with a lateral opening of width $b = 0.28$ m in one of the side walls. A lateral plane was attached to the flume in order to represent an inundation area. The entire set-up (flume and lateral plane) was placed at slopes equal to 0.1% in the x direction and 0.0% in the y direction respectively.

The Manning’s coefficient $n = 0.0105 \text{ m/s}^{1/3}$ suggested by [3] in the experiments was used for the bottom and the side walls. In particular, all the models were run using the same roughness coefficient which was not calibrated in this case. The initial condition is steady flow of $0.01 \text{ m}^3/\text{s}$ all over the channel and the boundary conditions consist of a constant inflow discharge of $0.01 \text{ m}^3/\text{s}$ at the inlet and critical flow at the outlet boundary. Water depths along the y direction were measured inside the flume just upstream the breach section by ultrasonic distance meters. The position of the probes as well as the topography of the test case are illustrated in Fig. 5.

In this work, numerical results obtained with two different strategies of coupling (frontal and lateral) are presented together with the numerical results obtained with a 2D model. The fully 2D mesh used for the computation is structured with 17390, 0.02×0.02 m squared elements. The lateral configuration is composed by the channel, represented by 200 cross sections spaced each 0.05 m and the flood plain, described by 9890 squared elements (0.02×0.02 m). In addition, a ‘double’ frontal coupling configuration is proposed: the channel is characterized by the 1D model for the first 5.28 m and for the last 3.94 m and the rest

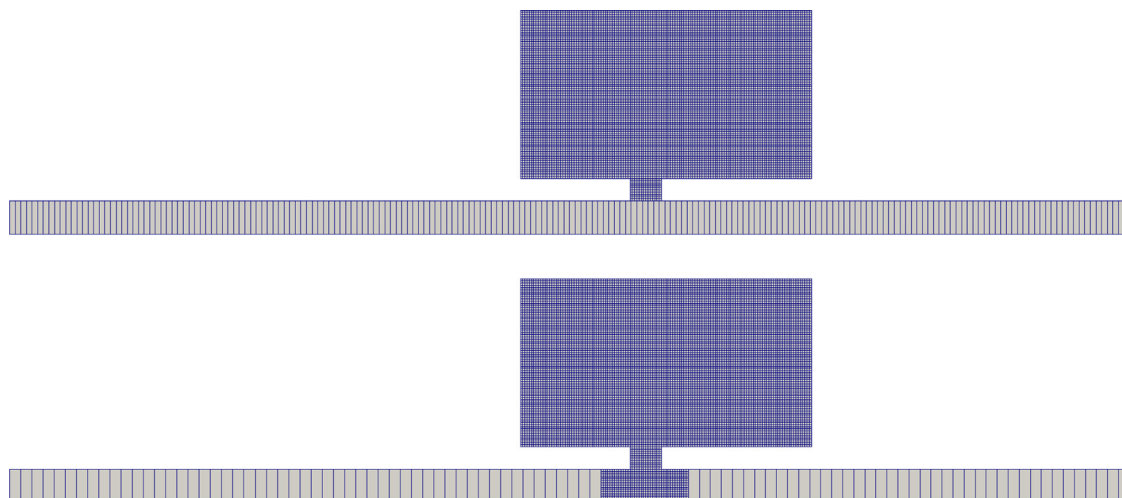


Fig. 6. Laboratory test case: 1D–2D lateral (upper) and frontal (lower) configurations.

Table 1

Laboratory test case: CPU time and speed up for each model.

Numerical model	CPU time (s)	Speed-up
1D–2D frontal	52.06	2.029
1D–2D lateral	51.80	2.039
2D	105.61	–

of the domain is modeled by a structured 2D grid of 0.02×0.02 m size (10475 squared cells). Fig. 6 shows the 1D–2D lateral and frontal configurations respectively.

The evolution in time in terms of water depth series is registered at each probe. The experimental observations are contrasted against the numerical results achieved by the fully 2D model, the 1D–2D lateral and frontal configuration in Fig. 7.

The lateral coupling approach is not able to reproduce the experimental elevations far from the gate opening, since in the position of the water gages the flume is modeled by 1D sections in which the water depth is assumed to be constant. Concerning the frontal configuration, the results are very similar to those obtained by the fully 2D model. As the only provided measurements are placed inside the main channel, the behavior of the schemes inside the floodplain can not be compared against experimental data. However, it is feasible to compare the numerical results achieved by the 1D–2D coupled (in both frontal and lateral configurations) against the same numerical results obtained by the complete 2D model. With this purpose, the evolution of time of water depth at points $P1P = (5.01, 1.59)$, $P2P = (6.75, 1.59)$, $P3P = (6.75, 0.85)$ and $P4P = (5.01, 0.85)$ (all of them inside the floodplain area) is plotted in Fig. 8. Moreover a snapshot of the system for the three schemes at time $t = 11.2s$ is shown in Fig. 9.

Although the results are slightly underestimated by the 1D–2D coupled model, the overall behavior is captured and the numerical solutions are comparable to that obtained by the 2D model. Regarding the snapshot, the frontal configuration seems to provide better results with respect to the 2D approach since the channel profile is well approximated. However, if focusing in the floodplain results, even the lateral configuration provides accurate and acceptable results. Therefore, it can be concluded that frontal configuration should be used if the interest is put on the variation across the main channel (in a junction, for example). Otherwise, the overall behavior far from the detail of the main river or channel is captured by both 1D–2D models.

The computational time consumed by each model is described in Table 1. Although they are in the order of seconds and the CPU time is very influenced by the preprocessing and the writing data process, both 1D–2D coupled configurations are able to halve the computational time with respect to the fully 2D model.

6. Application to the Tiber river flood simulation

6.1. Topography definition

Developments in GIS software and in computer processing allow the use of high-resolution DEMs in hydraulic simulations. Hydraulic variables like flow depth and velocity components can be highly variable over small spatial scales and, as such, are extremely sensitive to terrain parametrization in topography-based simulation models. Small errors in specifying bed elevation may have a large impact on the prediction of the flooding area.

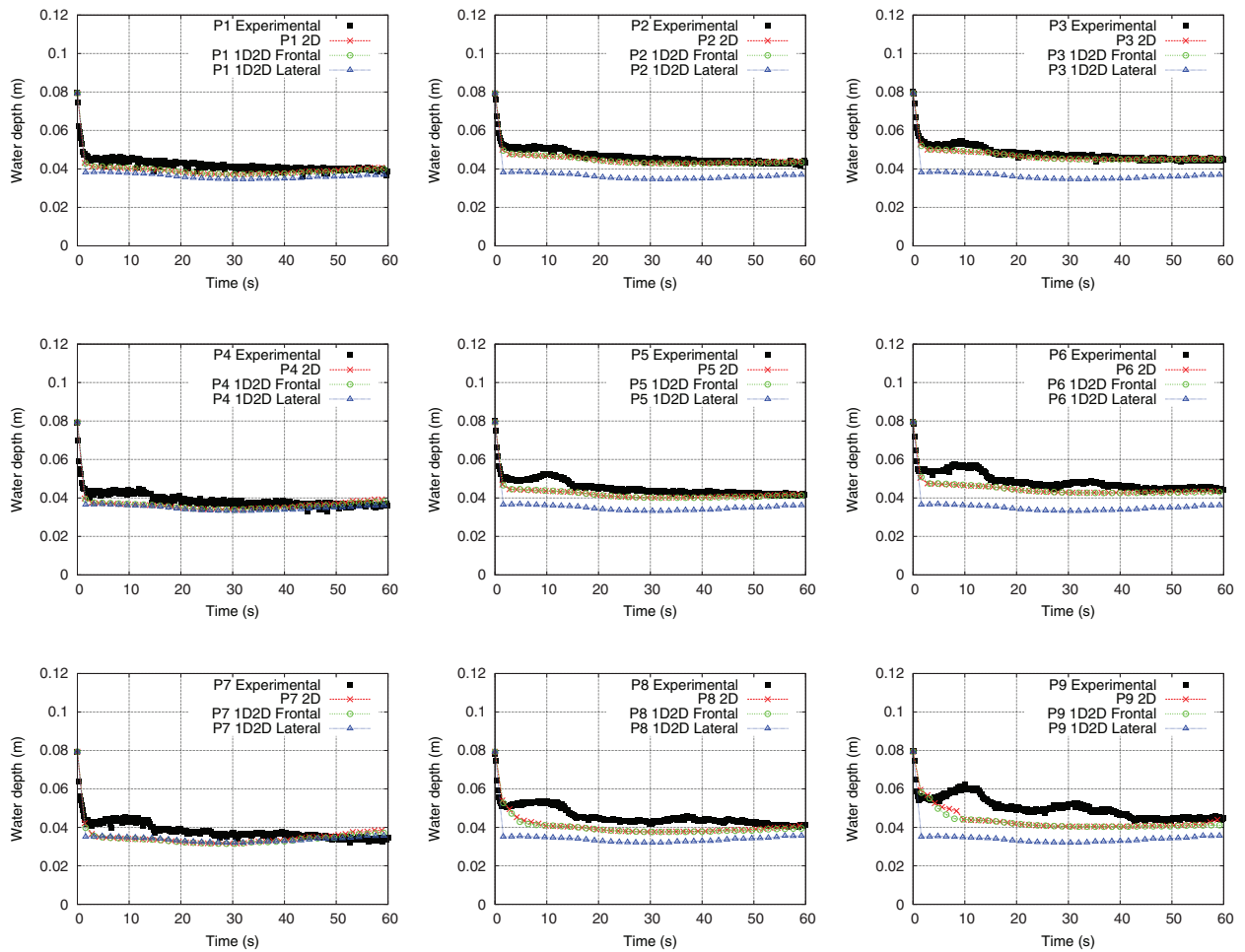


Fig. 7. Laboratory test case: comparison of numerical results and experimental measurements at probes P1 (upper left) to P9 (lower right).

The data available for this study were a digitized cartography (scale 1:10000) covering the bottom of the valley together with aerial photographs. Moreover a 2×2 m resolution digital elevation model (DEM) was also available together with 600 cross sections coming from land surveys. The topography used by the authors was obtained integrating the DEM with the land surveyed cross sections (10 for the considered reach displaced in orange in Fig. 10) in order to describe correctly the floodplain and the main channel.

The geometric description of the river channel and surrounding topography was essential for creating a computational mesh consistent with the surface of the study area. It can significantly affect the numerical results. In this case, first, the banklines were delineated to separate the river from the flooding area. Then, the 2D domain was built in order to guarantee the best match between land surveyed cross section in the river and DEM extracted cross sections. As an example, Fig. 11 shows a particular 1D cross section coming from the land survey and the corresponding one extracted by the modified DEM. Since the comparison is reasonable, the modified DEM was used in this work.

6.2. Tiber river flood

Tiber river is one of the most important Italian rivers: the catchment area at Rome is about 17000 km^2 . It is 406 km long, flowing from the Apennine Mountains to the Tyrrhenian Sea. Its mean discharge is $267 \text{ m}^3/\text{s}$ while the discharge for a return period of 200 years is $3200 \text{ m}^3/\text{s}$. For this study, a 6×2 km reach is considered, which will be referred to in what follows as the Ponzano reach. The flood here simulated occurred between the 27th of November and the 1st of December 2005. Its estimated return period is 50 years. The maximum discharge in the Ponzano reach was about $1440 \text{ m}^3/\text{s}$ and the surrounding area was almost completely flooded. As a result, several measurements were registered at different sections. Fig. 12 shows the inflow hydrograph (left) imposed as upstream boundary condition. The recorded evolution in time of the water level surface as well as the discharge at the outlet section were used to build the downstream boundary condition in the form of a gauging curve (see Fig. 12, right).

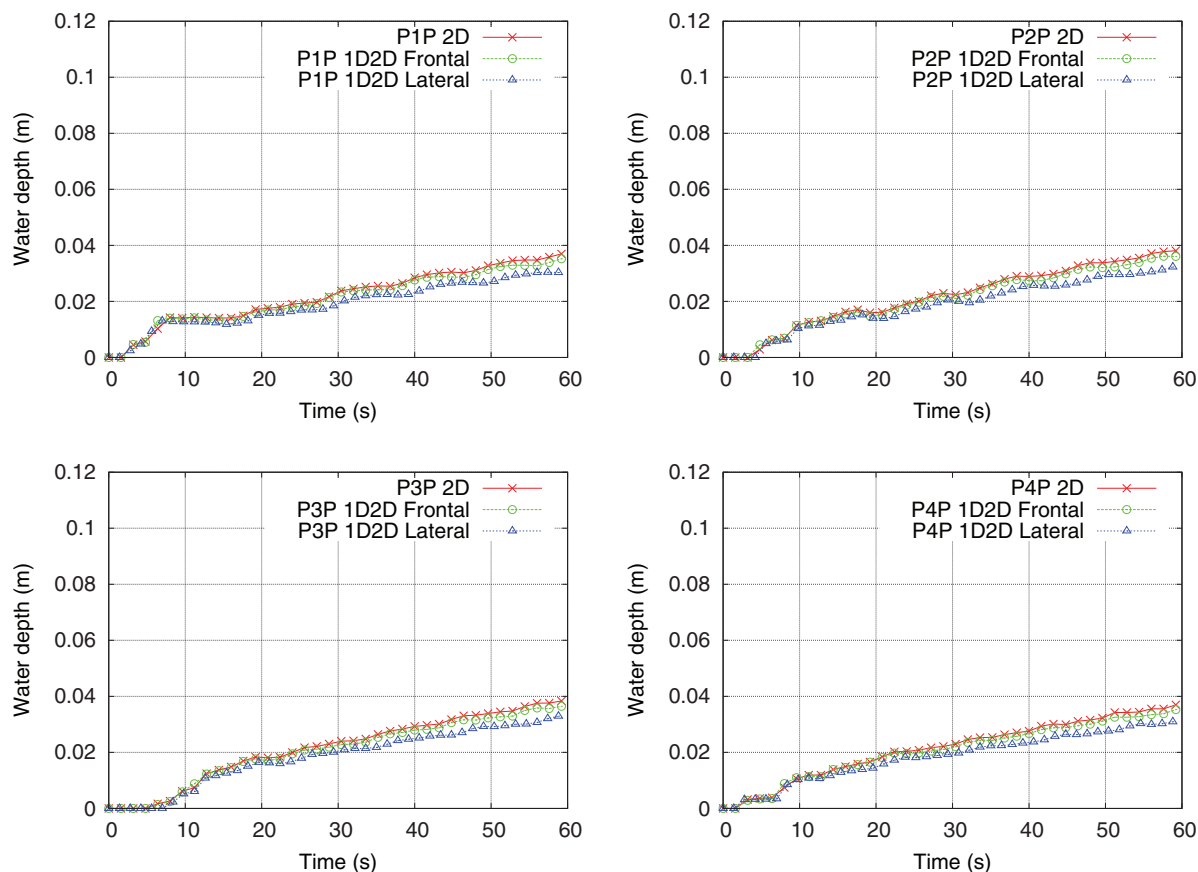


Fig. 8. Laboratory test case: comparison of numerical results and experimental measurements at probes P1P (upper left) to P4P (lower right).

The time evolution of the water surface elevation was measured in two sections in the Ponzano reach (S1 and S2), located inside the main channel. Besides the observed data, five probes were selected in order to compare all the proposed numerical models. The location of sections and probes as well as the topography of the Ponzano reach are shown in Fig. 13 (left).

In order to define homogeneous roughness areas, according to [2], two zones were defined: one for the main river with $n = 0.035 \text{ m/s}^{1/3}$ and the other one for the floodplain area with $n = 0.0446 \text{ m/s}^{1/3}$ (Fig. 13, right). No further calibration of the Manning coefficient value was performed as the focus of the present work is put on the relative performance of the models.

For the simulation of this event, two numerical models are used: a fully 2D numerical model and the suggested coupled 1D–2D model with a frontal and a lateral configuration. A fully two dimensional non structured domain made of 15,985 elements was first developed. As this domain describes poorly the main channel (even with only 2 elements), a refined mesh only in the main channel is used as reference, made of 26,895 elements. The 2D coarse mesh was then used to get the coupled lateral and frontal domains.

7. Discussion of the results

7.1. Local measurements and flooded area

The recorded water elevations in sections S1 and S2 are compared, in Fig. 14, with the numerical results on the fully coarse and refined 2D domain, and using the frontal and lateral coupling.

The numerical models can be also compared by using the information of the evolution in time of the water surface elevation registered on the probes P1–P5 (see Fig. 15).

The 1D–2D frontal model and the 2D coarse simulation generate almost the same results due to the fact that the 1D domain inside the frontal coupled configurations only covers a very small surface. Although the maximum peaks in water surface elevations are fairly captured, the peak times are not well reproduced by these models. In fact, the flooding wave comes earlier than the 2D fine and the 1D–2D coupled lateral configuration. This behavior is also observed at probes P1–P5 if compared to the 2D fine model. Additionally, the water surface elevations are always overestimated. This fact is possibly due to the bad representation

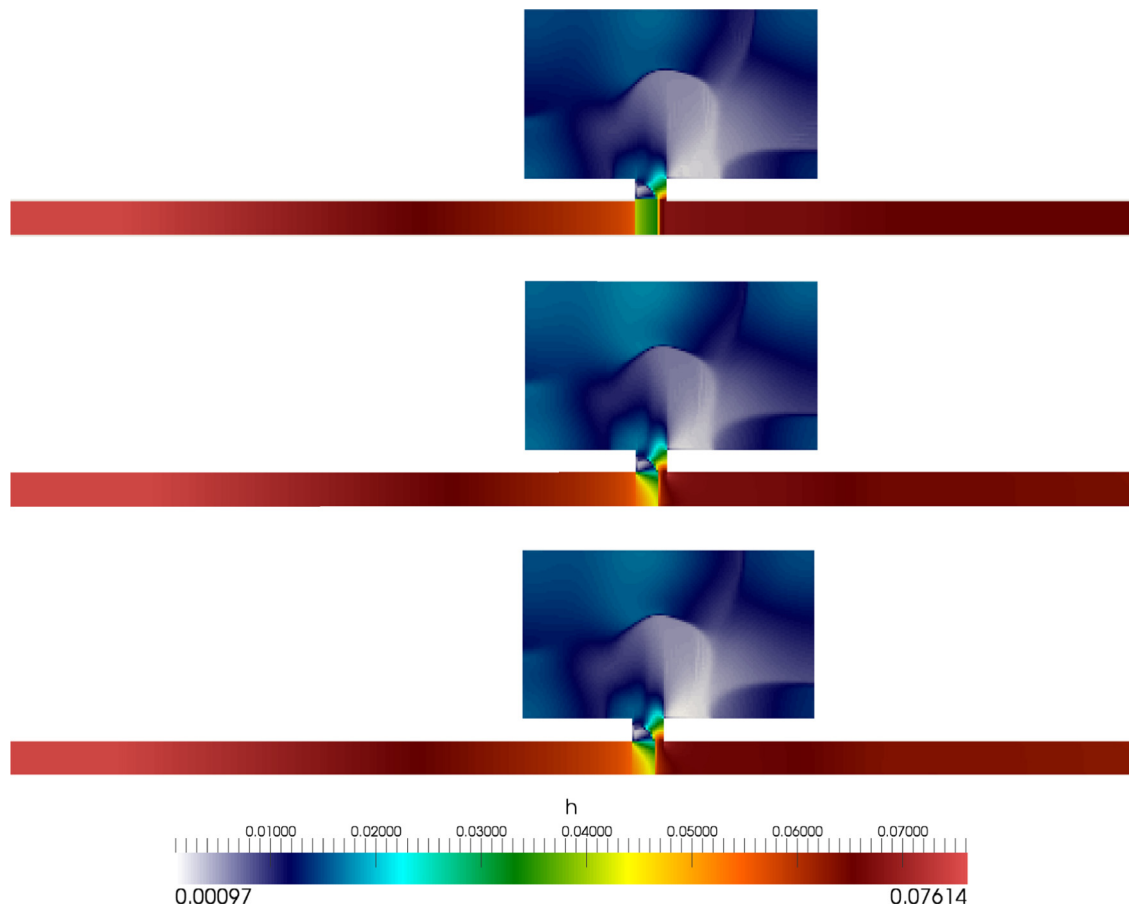


Fig. 9. Laboratory test case: snapshot at time $t = 11.2\text{ s}$ for the 1D–2D lateral, 1D–2D frontal and 2D models (from upper to lower respectively).

of the river bathymetry since a small number of elements discretize the main channel in both the 1D–2D frontal and the 2D coarse models.

The numerical results achieved by the fully 2D fine mesh are more accurate, although the water peaks in section S2 are not well reproduced. All models are unable to simulate well the observed data for section S2 so that it could be an effect of the downstream boundary condition, the Manning roughness coefficient (assumed constant along the main river) or even the bad representation of the bathymetry near this zone.

The 1D–2D coupled lateral model achieves reasonable results, compared to those obtained by the fully 2D fine mesh. It is worth emphasizing that the lateral coupling represents the main channel with 1D cross sections hence providing more reliable results than the 2D model if not appropriately discretized. In terms of timing both the 1D–2D lateral model and the 2D fine mesh model predict similar results at sections S1 and at all the observations points P1–P5. However, the water depth is sometimes underestimated (mainly probes P3 and P4).

This analysis is based on local measurements (sections and probes) along the domain. However, the differences can be estimated in terms of inundation maps generated by each numerical model. As an example, three snapshots during the flood at times $t = 33\text{ h}$, $t = 80\text{ h}$ and $t = 113\text{ h}$ (final state) are plotted at Figs. 16–18.

As can be observed, the flooding extension is almost well captured by all the schemes presented. In particular, the 1D–2D lateral configuration is able to reproduce appropriately the flooded area achieved by the reference solution, being partially overestimated with the fully 2D coarse mesh. In order to corroborate this hypothesis, the evolution in time of the flooded area (in km^2) computed by each model is plotted in Fig. 19. Although the lateral coupling underestimates the flooding area during the peak discharge, it is able to reproduce better the behavior achieved by the reference solution not only in terms of magnitude but also in terms of peak time accuracy.

7.2. Computational time

Attending to the cross comparisons displayed above, the use of a coupled 1D–2D numerical model has proved to be accurate with respect to the 2D numerical model, used as reference in absence of experimental data. Although the triangle cell areas far

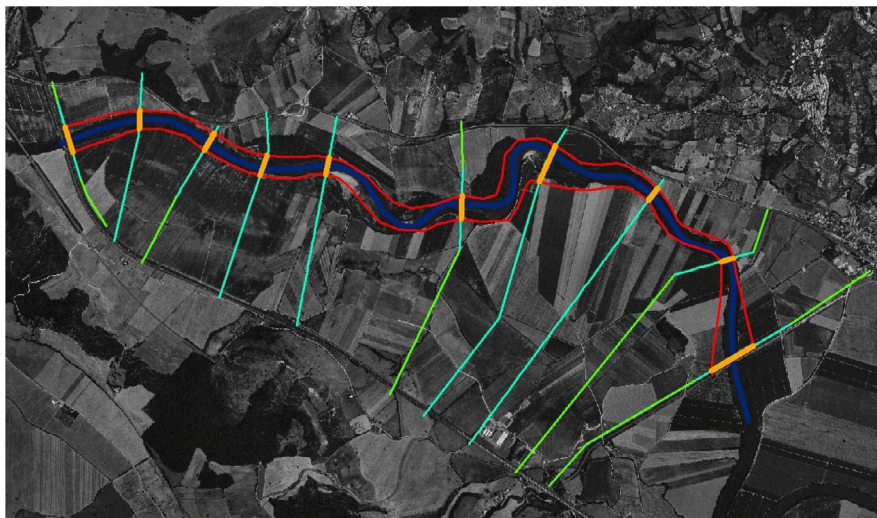


Fig. 10. Aerial photograph of Ponzano area with original and interpolated 1D cross sections.

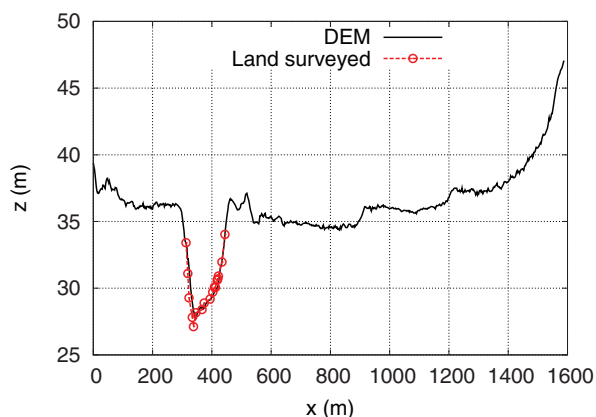


Fig. 11. Comparison between the land surveyed and the DEM reconstructed extraction for section 5 in Ponzano reach.

Table 2

Tiber river test case: CPU time and speed up for each model.

Numerical model	CPU time (s)	Speed-up
1D–2D frontal	2000.89	10.97
1D–2D lateral	1441.75	15.22
2D fine	21952.55	–

from the main river are the same and the uncertainties related to the discretization in the floodplains are removed, the 2D model requires a fine representation of the channel bathymetry to ensure correct results. Considering that the time step is governed ultimately by the cell sizes of the domain, the use of a 1D–2D coupled model should reduce considerably the computational time. In fact, not only the time step size is enlarged when using a 1D–2D lateral coupled model, but also the cells discretizing the main river domain are eliminated of the computation, achieving a double gain.

Table 2 shows the CPU time consumed by each model and the gain in terms of speed-up's of the 1D–2D coupled model with respect to the 2D refined model.

A significant reduction in the computational time is observed when using a 1D–2D coupled model. In particular, the lateral configuration, which achieved better results is able to carry out the simulation 15 times faster than the fully 2D model. A similar gain could be obtained by parallelizing the 2D code on distributed memory architectures using MPI, on the most common shared memory processors by means of OpenMP [24] or even using the more recent paradigms such as GPU computing [25]. However, the proposed 1D–2D model can also be parallelized adopting the same techniques, and the speed-up's should scale accordingly in the 1D–2D model. It is worth noting that all the simulations were carried out in a Intel Core 2 Duo Quad Core Q9550 2.83 GHz.

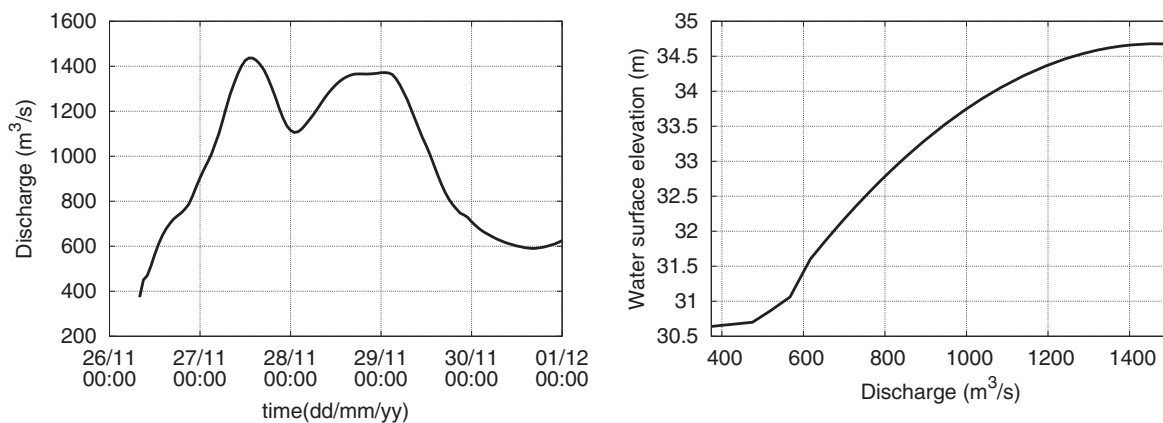


Fig. 12. Ponzano reach: upstream (left) and downstream (right) boundary conditions.

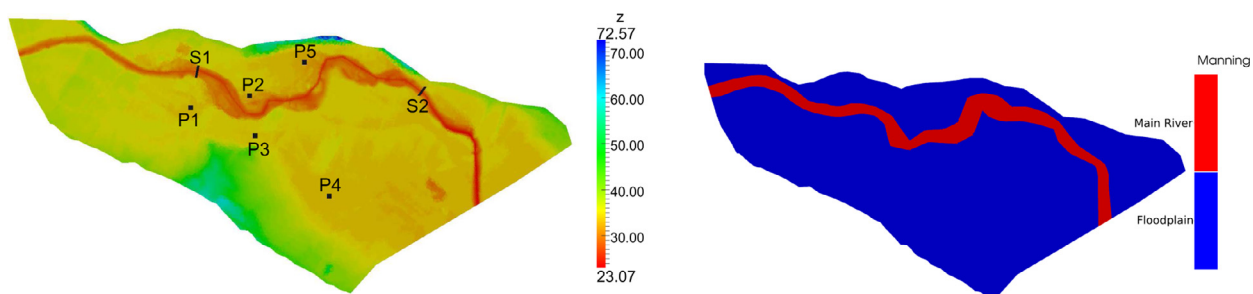


Fig. 13. Ponzano reach: topography and location of sections and probes (left) and Manning roughness map (right).

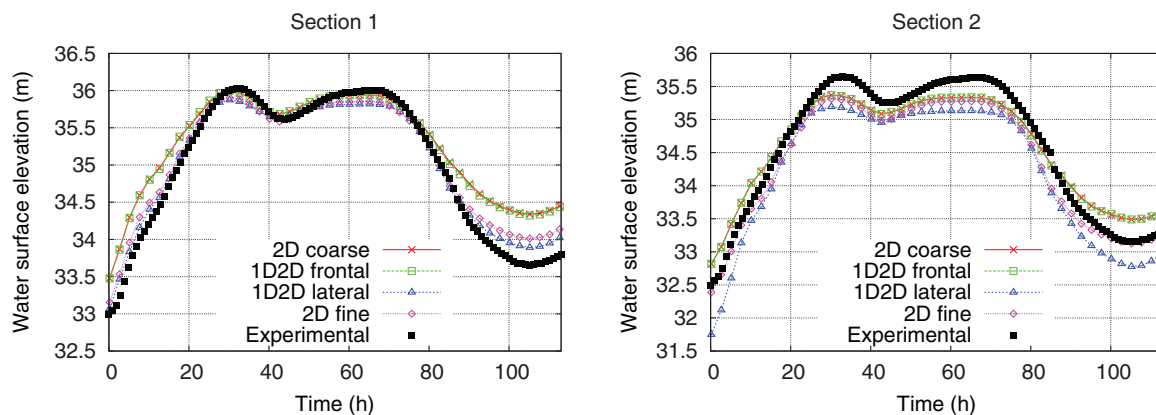


Fig. 14. Ponzano reach: comparison between measured and computed data for sections S1 and S2.

8. Conclusions

A 1D–2D coupled model has been presented for predicting flood inundation in river basins. Both 1D and 2D models are implemented in a finite volume framework, using an explicit first order upwind numerical scheme based on Roe's linearization. The coupling zone has been generalised to complex problems that may be encountered in realistic applications. This requirement implies a suitable meshing procedure, able to achieve a perfect match between the 1D and the 2D domains that are geometrically coupled.

The models are dynamically linked using exclusively information from the computational cells, without any extra condition. In order to couple the models, two strategies are extended this work, based on Conserving Mass (OMC) or Mass and Momentum (MMC), respectively. The computation of the fully mass and momentum conservation is carefully carried out by means of the information that is exchanged through the computational edges or interfaces that separates both models. Therefore, the choice

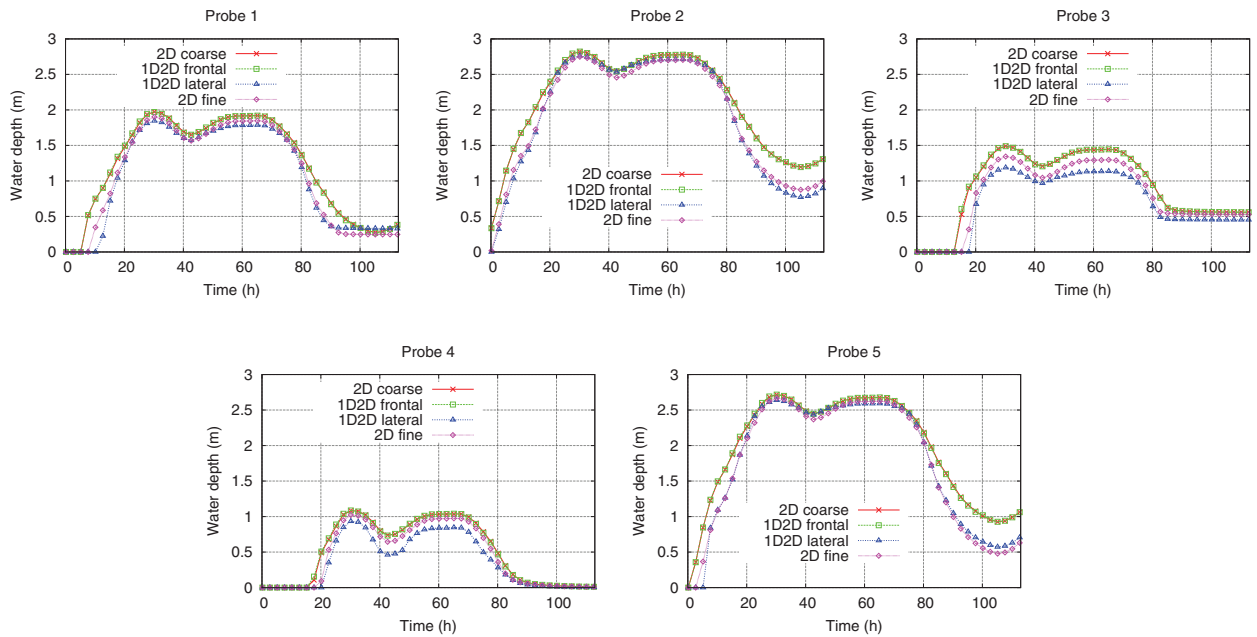


Fig. 15. Ponzano reach: comparison among the different numerical models at probes P1–P5.

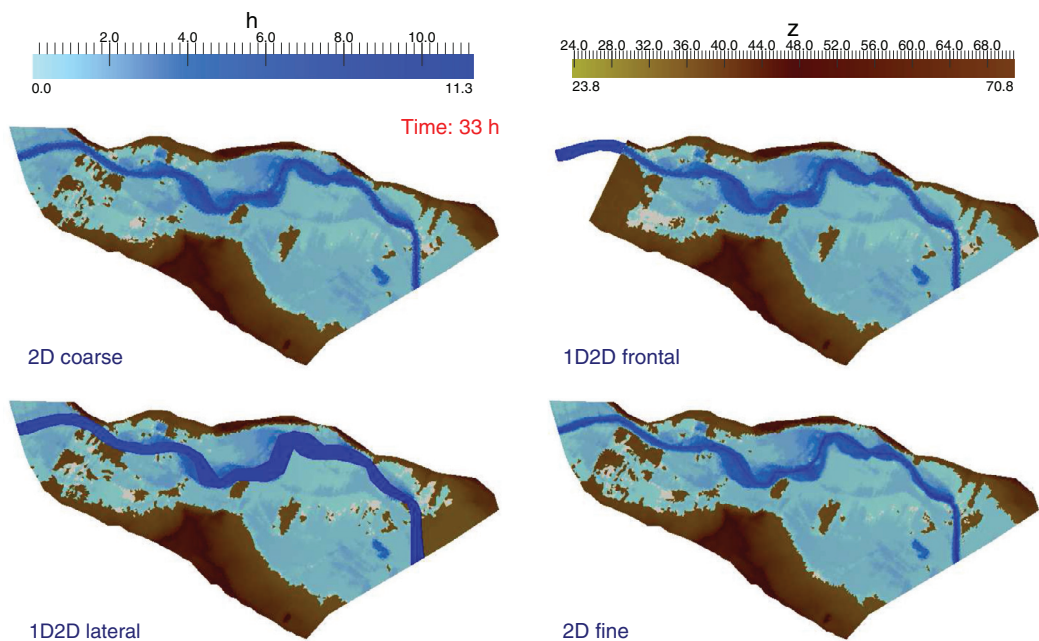


Fig. 16. Ponzano reach: flooded area at time $t = 33$ h. computed by the 2D coarse (upper left), 1D–2D frontal (upper right), 1D–2D lateral (lower left) and 2D fine model (lower right).

of the local adequate strategy will be closely related to the number of boundary conditions to be imposed and the flow regime that takes place at each coupling zone.

In irregular geometries, it is necessary to define exactly the location and the moment of overflow occurrence that triggers the connection between the models. Consequently, left and right overflow levels have to be constructed for each coupling zone. On the other hand, the correct distribution of the water volumes between the models is performed by means of hydraulic tables that accounts for the variability not only in the bathymetry of the 1D cross sections but also in the elevations of the 2D cells. This fact will ensure a perfect well-balancing for the 1D–2D coupled model.

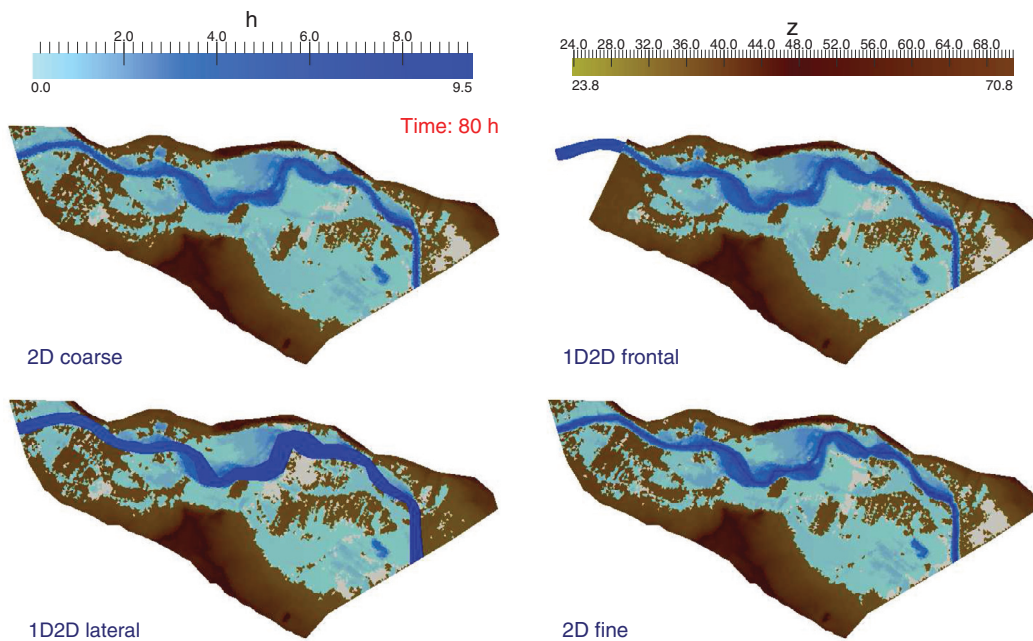


Fig. 17. Ponzano reach: flooded area at time $t = 80$ h. computed by the 2D coarse (upper left), 1D–2D frontal (upper right), 1D–2D lateral (lower left) and 2D fine model (lower right).

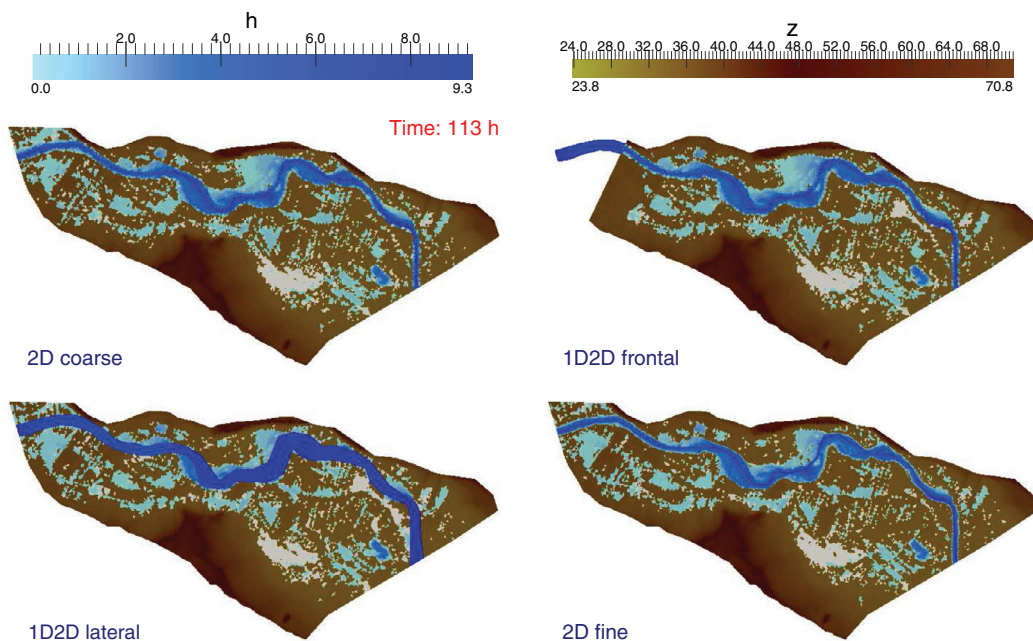


Fig. 18. Ponzano reach: flooded area at time $t = 113$ h. computed by the 2D coarse (upper left), 1D–2D frontal (upper right), 1D–2D lateral (lower left) and 2D fine model (lower right).

The model has been tested for a levee breaking laboratory experiment and then applied to the Tiber river near the urban area of Rome (Italy). Different meshes have been used for the discretization of the domain: structured and unstructured ones. Numerical results have been compared with a fully 2D model as well as with experimental and field measurements when possible.

In the laboratory test case, when representing the domain with a 1D model (inside a 1D–2D lateral configuration), the two dimensional features within the channel are not well captured. However, when regarding the propagation into the lateral floodplain, the numerical results are satisfactorily captured. Besides, the 2D model represents correctly such features. Also the 1D–2D frontal coupling gives very similar results in comparison to the 2D simulation.

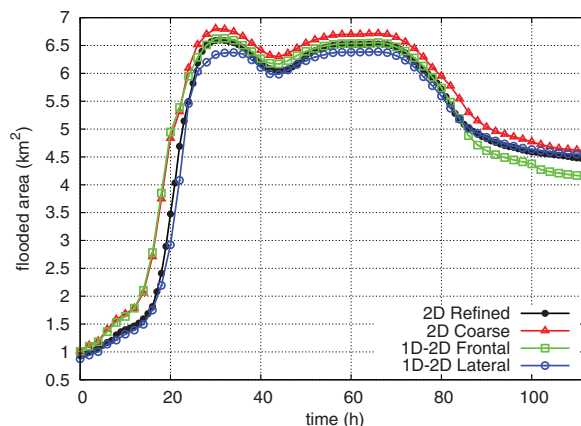


Fig. 19. Ponzano reach. Time evolution of the flooded area computed by each model.

The simulation of a flooding event in a river reach of the Tiber river has been next performed. Field measurements were available at different locations and the results achieved by the coupled model (frontal and lateral) are compared to those obtained by a fully 2D model (coarse and fine meshes). Also the flooding extension is evaluated using inundation maps. The frontal 1D–2D model achieves similar results to the fully 2D model. However, the restriction of using a time step governed by the 2D cells inside the river together with the difficulty of choosing where the 1D model ends up, makes this option not as attractive as the 1D–2D coupled model with lateral configuration.

In conclusion, the frontal coupling offers the possibility to model in 2D a river reach or a channel. This is useful if detailed information across the channel/river section is required (i.e., when modelling a junction) and a very fine mesh is used inside the channel/river. In the case of real world applications, the 1D–2D lateral configuration becomes a good option. First, the correct flooding propagation in the river bed is ensured by means of 1D cross sections that prevent the use of a 2D fine discretization. On the other hand, the flow developed inside the adjacent floodplain areas is well captured in the 2D domain out of the river channel. Furthermore, a reduction in the computational time with respect to the fully 2D model is confirmed, achieving speed-ups of around 15 ×.

Acknowledgments

This research was supported by the projects HI2006/0152 and IT0787H845, financed by the Spanish Ministry of Education and Science and by the Italian Ministry of Education, University and Research (respectively).

References

- [1] G.R. Aggett, J.P. Wilson, Creating and coupling a high resolution DTM with a 1D hydraulic model in a GIS for scenario-based assessment of avulsion hazard in a gravel bed river, *Geomorphology* 113 (2009) 21–34.
- [2] G. Arcement, V. Schneider, 1989, Guide for Selecting Mannings Roughness Coefficients for Natural Channels and Flood Plains. U.S. Geological Survey Water Supply Paper 2339.
- [3] F. Aureli, P. Mignosa, Rapidly varying flows due to levee-breaking. *Proceedings of Riverflow 2002*, Louvain La Neuve 1 (2002) 459–466.
- [4] E. Bladé, M. Gomez-Valentín, J. Dolz, Quasi-two dimensional modelling of flood routing in rivers and flood plains by means of storage cells. A: “modelling of flood propagation over initially dry areas”, *ASCE* (1994) 156–170.
- [5] S.F. Bradford, B.F. Sanders, Finite-volume model for shallow-water flooding of arbitrary topography, *J. Hydraulic Eng.* 128 (3) (2002) 289–298.
- [6] P. Brufau, M.E. Vázquez Cendón, P. García Navarro, A numerical model for the flooding and drying of irregular domains, *Int. J. Numer. Meth. Fluids* 39 (2002) 247–275.
- [7] P. Brufau, P. García-Navarro, E. Vázquez-Cendón, Zero mass using un steady wetting-drying conditions in shallow flows over dry irregular topographies, *Int. J. Numer. Methods Fluids* 45 (2004) 1047–1082.
- [8] J. Burguete, P. García-Navarro, Efficient construction of high-resolution TVD conservative schemes for equations with source terms: application to shallow water flows, *Int. J. Numer. Methods Fluids* 37 (2) (2001) 209–248.
- [9] A. Castellarin, A. Domeneghetti, A. Brath, Identifying robust large scale flood risk mitigation strategies: a quasi 2D hydraulic model as a tool for the Po River, *Phys. Chem. the Earth* 36 (2011) 299–308.
- [10] D. Caviedes-Voullième, M. Morales-Hernández, I. López-Marjuan, P. García-Navarro, Reconstruction of 2D river beds by appropriate interpolation of 1D cross-sectional information for flood simulation, *Environ. Model. Softw.* 61 (2014) 206–228.
- [11] Y. Chen, Z. Wang, Z. Liu, D. Zhu, 1D-2D coupled numerical model for shallow water flows, *J. Hydraulic Eng.* 138 (2) (2012) 122–132.
- [12] W.B. Chen, W.C. Liu, C.Y. Wu, Coupling of a one-dimensional river routing model and a three-dimensional ocean model to predict overbank flows in a complex river-ocean system, *Appl. Math. Model.* 37 (9) (2013) 6163–6176.
- [13] D.M. Cobby, D.C. Mason, M.S. Horritt, P.D. Bates, Two-dimensional hydraulic flood modelling using a finite-element mesh decomposed according to vegetation and topographic features derived from airborne scanning laser altimetry, *Hydrological Proces.* 17 (10) (2003) 1979–2000.
- [14] J.A. Cunge, Two dimensional modelling of floodplains, *Unsteady Flow in Open Channels*, Water resources publications, Fort Collins, 1975, pp. 705–762.
- [15] J.F. Dhondia, G.S. Stelling, Application of one dimensional two dimensional integrated hydraulic model for flood simulation and damage, in: *Proceedings of the 5th International Conference on Hydroinformatics*, Cardiff, 2002, pp. 265–276.
- [16] G. Di Baldassarre, A. Castellarin, A. Montanari, A. Brath, Probability weighted hazard maps for comparing different flood risk management strategies: a case study, *Natural Hazards* 50 (2009) 479–496.

- [17] E.D. Fernandez-Nieto, J. Marin, J. Monnier, Coupling superposed 1D and 2D shallow water models: source terms in finite volume schemes, *Comput. Fluids* 39 (2010) 1070–1082.
- [18] P. Finaud-Guyot, C. Delenne, V. Guinot, C. Llovel, 1D-2D coupling for river flow modelling, *Comptes Rendus Mecanique* 339 (2011) 226–234.
- [19] I.Y. Gejadze, J. Monnier, On a 2D zoom for the 1D shallow water model: coupling and data assimilation, *Comput. Methods Appl. Mech. Eng.* 196 (2007) 4628–4643.
- [20] M. Gregory, B. Walker, S. Yi, B. Cunningham, J. Kjelds, Case studies in automated floodplain mapping, in: *Proceedings of Flood management ASCE conference Urban Drainage Modeling*, 2001, pp. 367–375.
- [21] K.Y. Han, J.T. Lee, J.H. Park, Flood inundation analysis resulting from levee break, *J. Hydraulic Res.* 36 (5) (1998) 747–759.
- [22] M.S. Horritt, P.D. Bates, Predicting floodplain inundation: Raster-based modelling versus the finite-element approach, *Hydrological Proces.* 15 (5) (2001) 825–842.
- [23] S.N. Kuiry, D. Sen, P.D. Bates, Coupled 1D- quasi 2D flood inundation model with unstructured grids, *J. Hydraulic Eng.* 136 (8) (2010) 493–506.
- [24] A. Lacasta, P. García-Navarro, J. Burguete, J. Murillo, Preprocess static subdomain decomposition in practical cases of 2D unsteady hydraulic simulation, *Comput. Fluids* 80 (0) (2013) 225–232.
- [25] A. Lacasta, M. Morales-Hernández, J. Murillo, P. García-Navarro, An optimized GPU implementation of a 2D free surface simulation model on unstructured meshes, *Adv. Eng. Softw.* 78 (0) (2014) 1–15.
- [26] B. Lin, J.M. Wicks, R.A. Falconer, K. Adams, Integrating 1D and 2D hydrodynamic models for flood simulation, in: *Proceedings of the Institution of Civil Engineers, Water Management*, 159, 2006, pp. 19–25.
- [27] J. Marin, J. Monnier, Superposition of local zoom models and simultaneous calibration for 1D-2D shallow water flows, *Math. Comput. Simul.* 80 (2009) 547–560.
- [28] A. Masoero, P. Claps, N.E.M. Asselman, E. Mosselman, G. Di Baldassarre, Reconstruction and analysis of the Po River inundation of 1951, *Hydrological Proces.* 27 (9) (2013) 1341–1348.
- [29] H.K. McMillan, J. Brasington, Reduced complexity strategies for modelling urban floodplain inundation, *Geomorphology* 90 (2007) 226–243.
- [30] E. Miglio, S. Perotto, F. Saleri, Model coupling techniques for free surface flow problems: Part I, *Nonlin. Anal.* 63 (2005) 1885–1896.
- [31] M. Morales-Hernández, P. García-Navarro, J. Burguete, P. Brufau, A conservative strategy to couple 1D and 2D models for shallow water flow simulation, *Comput. Fluids* 81 (2013) 26–44.
- [32] J. Murillo, P. García-Navarro, Weak solutions for partial differential equations with source terms: application to the shallow water equations, *J. Comput. Phys.* 229 (2010) 4327–4368.
- [33] J. Murillo, P. García-Navarro, J. Burguete, Time step restrictions for well-balanced shallow water solutions in non-zero velocity steady states, *Int. J. Numer. Meth. Fluids* 60 (2009) 1351–1377.
- [34] G. Petaccia, F. Savi, Numerical modelling of shock waves: simulation of a large number of laboratory experiments, in: *Proceedings of International Conference in Fluvial Hydraulics, Riverflow*, 1, 2002, pp. 449–458.
- [35] G. Petaccia, L. Natale, F. Savi, M. Velickovic, Y. Zech, S. Soares-Frao, Flood wave propagation in steep mountain rivers, *J. Hydroinform.* 15 (1) (2013) 120–137.
- [36] J.W.F. Remo, N. Pinter, R. Heine, The use of retro and scenario modeling to assess effects of 100 + years river of engineering and land cover change on middle and lower Mississippi flood stages, *J. Hydrology* 376 (2009) 403–416.
- [37] P.L. Roe, Approximate Riemann solvers, parameter vectors and difference schemes, *J. Comput. Phys.* 43 (1981) 357–372.
- [38] A. Verwey, Latest development in floodplain modelling-1D/2D integration, *Proceedings of the Australian Conference on Hydraulics in Civil Engineering*, The Institute of Engineers, Hobart, 2001, pp. 13–24.
- [39] I. Villanueva, N.G. Wright, Linking Riemann and storage cell models for flood prediction, in: *Proceedings of the Institution of Civil Engineers, Water Management*, 159, 2006, pp. 27–33.
- [40] N.G. Wright, I. Villanueva, P.D. Bates, D.C. Manson, M.D. Wilson, G. Pender, S. Neelz, Case study of the use of remotely sensed data for modelling flood inundation on the river Severn, UK, *J. Hydrologic Eng.* 134 (5) (2008) 533–540.
- [41] J. Yin, D. Yu, Z. Yin, J. Wang, S. Xu, Multiple scenario analyses of Huangpu River flooding using a 1D/2D coupled flood inundation model, *Nat. Hazards* 66 (2013) 577–589.
- [42] D. Yu, S.N. Lane, Coupled modelling of flood inundation over a topographically complex urban floodplain, *Geophys. Res. Abs.* 9 (2007).